Journal of Geophysical Research: Atmospheres

RESEARCH ARTICLE
10.1029/2018JD028719

Simulation of Longwave Enhancement in Boreal and Montane Forests

M. Todt[1], N. Rutter[1], C. G. Fletcher[2], L. M. Wake[1], P. A. Bartlett[3], T. Jonas[4], H. Kropp[5], M. M. Loranty[5], and C. Webster[4,6]

[1]Department of Geography, Northumbria University, Newcastle upon Tyne, UK, [2]Department of Geography and Environmental Management, University of Waterloo, Waterloo, Ontario, Canada, [3]Climate Research Division, Environment and Climate Change Canada, Toronto, Ontario, Canada, [4]WSL Institute for Snow and Avalanche Research SLF, Davos Dorf, Switzerland, [5]Department of Geography, Colgate University, Hamilton, NY, USA, [6]School of GeoSciences, University of Edinburgh, Edinburgh, UK

Abstract Boreal forests cover about a fifth of seasonally snow-covered land over the Northern Hemisphere. Enhancement of longwave radiation beneath coniferous forests has been found to impact the surface energy balance and rates of snowmelt. Although the skill of model-simulated snowmelt has been shown to be lower for forests than for open areas, model intercomparisons and evaluations of model parameterizations have not yet focused on longwave enhancement. This study uses stand-scale forcing for the simulation of subcanopy longwave radiation by Community Land Model version 4.5 (CLM4.5) and to drive SNOWPACK, a snow model featuring more complex canopy structure, as a benchmark model for CLM4.5. Simulated subcanopy longwave radiation and longwave enhancement are assessed using measurements from forest stands located within perennially snow-covered regions. These forest stands, of varying canopy density, cover the range of boreal plant functional types in CLM4.5. CLM4.5 is found to overestimate the diurnal range of subcanopy longwave radiation and longwave enhancement, and simulation errors increase with decreasing cloudiness and increasing vegetation density. Implementation of a parameterization of heat storage by biomass reduces simulation errors but only marginally affects the amplitude of diurnal ranges. These results reaffirm previous findings that simulation of subcanopy longwave radiation can be improved by partitioning the vegetation canopy into two layers. Moreover, this study reveals the variations of simulation errors across meteorological conditions and vegetation density, the latter of which is the most important parameter for longwave enhancement independent of vegetation type.

Key Points:
- Simulation of subcanopy LWR by CLM4.5 was assessed during snowmelt season at forest stands with varying vegetation density and types
- Diurnal ranges of subcanopy LWR and LW enhancement are overestimated by CLM4.5 with errors increasing for clearer sky and denser vegetation
- Comparison to SNOWPACK suggests addition of a two-layer vegetation effect is necessary to reduce overestimated range of LW enhancement

Supporting Information:
- Supporting Information S1

Correspondence to:
M. Todt,
markus.todt@northumbria.ac.uk

Citation:
Todt, M., Rutter, N. J., Fletcher, C. G., Wake, L., Bartlett, P. A., Jonas, T., et al. (2018). Simulation of longwave enhancement in boreal and montane forests. *Journal of Geophysical Research: Atmospheres*, *123*. https://doi.org/10.1029/2018JD028719

Received 16 APR 2018
Accepted 26 NOV 2018
Accepted article online 7 DEC 2018

Author Contributions

Conceptualization: M. Todt, N. Rutter, C. G. Fletcher
Data curation: P. A. Bartlett, T. Jonas, H. Kropp, M. M. Loranty, C. Webster
Methodology: M. Todt
Writing - Original Draft: M. Todt
Formal Analysis: N. Rutter
Visualization: M. Todt
Writing - review & editing: N. Rutter, C. G. Fletcher, L. M. Wake, P. A. Bartlett, T. Jonas, H. Kropp, M. M. Loranty, C. Webster

1. Introduction

Observed Northern Hemisphere (NH) spring snow cover extent (SCE) has declined rapidly since the start of the 21st century at a rate faster than that for annual minimum sea ice extent (Derksen & Brown, 2012). This decline in SCE is projected to continue, or even accelerate, over the remainder of the 21st century (Brutel-Vuilmet et al., 2013; Thackeray et al., 2016). Yet, significant challenges persist in the representation of SCE in the current generation of climate models; both the observed trend and interannual variability of spring SCE exceed the range of historical simulations from the Climate Model Intercomparison Project's fifth phase suite of models, reducing confidence in future projections (Brutel-Vuilmet et al., 2013; Derksen & Brown, 2012; Mudryk et al., 2014; Rupp et al., 2013; Thackeray et al., 2016).

Imperfect model physics and intermodel spread may partly be due to modeling of processes within boreal forests, which are estimated to make up almost one fifth of the NH seasonally snow-covered region (Rutter et al., 2009). Snow Model Intercomparison Project's second phase displayed higher modeling skill for open than for forested sites, which was attributed to more complex snow processes in forested areas (Essery et al., 2009; Rutter et al., 2009). The impact of forest cover on surface energy fluxes is manifold, especially in the presence of snow. The most significant influence is via the reduction of surface albedo, where the darker canopy vegetation masks the bright snow surface beneath (Essery, 2013; Thackeray et al., 2014). Forest canopy also intercepts snowfall, causing a temporary spike in albedo, which reverts back to darker canopy albedo after snow is removed through unloading or sublimation. Suppressed turbulent mixing beneath the canopy causes forests to act as cold air sinks (Link & Marks, 1999; Webster et al., 2016a).

One additional process is the effect of vegetation on longwave radiation fluxes below the canopy. Due to its low albedo, the canopy absorbs a substantial amount of solar radiation and accordingly emits longwave radiation toward the ground, which frequently exceeds atmospheric longwave radiation. This process is called longwave enhancement and potentially contributes to ripening or melting of snow cover. Extensive observations of subcanopy longwave radiation in dense subalpine and alpine forests by Webster et al. (2016a; 2016b) revealed longwave enhancement values of up to 1.5, or 150%, and net longwave radiation fluxes into snow reaching 10-min averages of up to 40 W/m^2 during clear-sky days in spring. In contrast, net longwave radiation fluxes of about −100 W/m^2 are typical for snow under clear-sky conditions in unforested areas. Positive net longwave radiation fluxes are due to snow surface temperature being limited to 0 °C while vegetation temperatures increase with increasing solar elevation angle and season, indicating that longwave enhancement is a crucial process prior to or during snowmelt. Similar contrasts in surface net longwave radiation between forested and unforested sites have been observed for evergreen Canadian boreal forests (Ellis et al., 2010; Harding & Pomeroy, 1996), and vegetation enhancing snowmelt has been reported for a subarctic open woodland during overcast days and early in the snowmelt season when solar elevation angles were low (Woo & Giesbrecht, 2000). The impact of forest coverage on snowmelt varies regionally depending on forest density and climate as the respective contributions by shortwave and longwave radiation change throughout the snowmelt season (Lundquist et al., 2013; Sicart et al., 2004; Strasser et al., 2011) and meteorological conditions impact both atmospheric longwave radiation and vegetation temperatures (Pomeroy et al., 2009; Sicart et al., 2004). The impact of longwave enhancement on timing of snowmelt illustrates the potential importance of this process on large-scale simulations.

Physical representation of tree components is important to accurately simulate variations in vegetation temperatures and longwave emittance, especially during periods of high insolation when trunks exhibit higher temperatures than both needles and air (Pomeroy et al., 2009; Webster et al., 2016a). Gouttevin et al. (2015) improved the simulation of subcanopy longwave radiation in a snow cover model (SNOWPACK) by increasing the complexity of canopy representation. Although several studies have demonstrated the enhancement of longwave radiation beneath forest canopies (Essery et al., 2008; Howard & Stull, 2013; Lundquist et al., 2013; Pomeroy et al., 2009; Rowlands et al., 2002; Sicart et al., 2004; Webster et al., 2016a), as yet there has been no effort to assess simulation of this process by global climate models. Model intercomparisons have used offline simulations, that is, uncoupled model components, or extensive point-scale forcing data (Henderson-Sellers et al., 1995; Rutter et al., 2009), while success in increasing process-level understanding was achieved by focusing on and comparing forest albedo masking or specific snow parameterizations (Essery, 2013; Essery et al., 2013; Lafaysse et al., 2017). A similar approach was used in this study by creating a toy model to simulate forest stand-scale subcanopy longwave radiation by Community Land Model version 4.5 (CLM4.5), a component of Community Earth System Model that was part of the Climate Model Intercomparison Project's fifth phase (Gent et al., 2011), and to compare CLM4.5 with SNOWPACK. This approach uses these models outside of their parent model frameworks enabling application of the same stand-scale forcing data and simplifying comparison, modification, and tracking of the effect of changes. In response to the essentially unknown accuracy of longwave enhancement in global climate models, this study aims to assess the simulation of longwave enhancement by CLM4.5 across varying vegetation types and densities. Consequently, the objectives of this study are the following:

a. to present an overview of measurements of subcanopy longwave radiation and longwave enhancement across forests of different vegetation types and densities;
b. to construct a toy model to use stand-scale observations for evaluation of simulation of subcanopy longwave radiation and longwave enhancement by CLM4.5 and direct comparison to subcanopy longwave radiation simulated by SNOWPACK; and
c. to evaluate the addition of a biomass heat storage parameterization within CLM4.5.

Simulation of subcanopy longwave radiation by CLM4.5 and SNOWPACK as well as the Toy Model are described in section 2. Forest stand sites and forcing and evaluation data are presented in section 3. Evaluation results are given in section 4, and their implications are discussed in section 5.

2. Modeling Subcanopy Longwave Radiation

Longwave enhancement is the process of vegetation changing, usually increasing, longwave radiation reaching the ground relative to atmospheric forcing and is quantified by the ratio of below-canopy to above-canopy

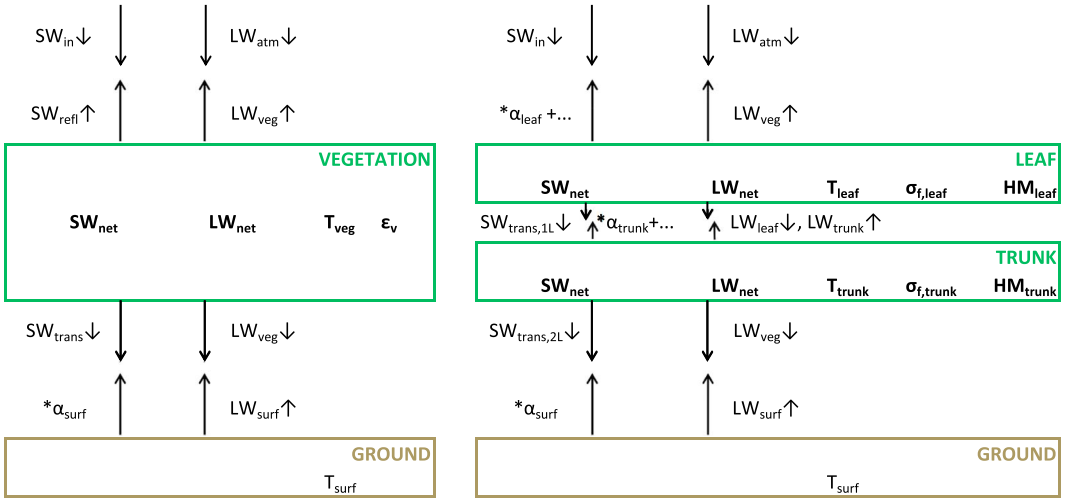

Figure 1. Radiation schemes of the big-leaf approach used in CLM4.5 (left) and interactive two-layer vegetation canopy used in SNOWPACK (right). Figures are adapted from Oleson et al. (2013) and Gouttevin et al. (2015), respectively. Dots "..." denote multiple reflections of shortwave radiation between layers in SNOWPACK. Note that $LW_{veg}\uparrow$ and $LW_{veg}\downarrow$ are equal by design in CLM4.5 but not in SNOWPACK, due to differing contributions from the vegetation layers. Also, $LW_{veg}\downarrow$ differs between CLM4.5 and SNOWPACK as seen in equations (2) and (7).

longwave radiation. Although generally larger than 1, longwave enhancement values can be smaller when cloud cover increases atmospheric longwave radiation and limits insolation. Since atmospheric longwave radiation is an input variable to land surface models, from either observations or an atmospheric model, simulated longwave enhancement depends on simulated subcanopy longwave radiation and is thus directly linked to vegetation surface temperatures via the Stefan-Boltzmann law.

2.1. CLM4.5

A technical description of CLM4.5 is given by Oleson et al. (2013), and the radiation scheme for vegetation is displayed in Figure 1. Vegetation in CLM4.5 is parameterized as a single layer using a big-leaf approach. Generally, subcanopy longwave radiation LW_{sub} is a weighted sum of atmospheric longwave radiation LW_{atm} and longwave radiation emitted by vegetation LW_{veg}. In CLM4.5, vegetation emissivity ε_v used for weighting depends on leaf area index (LAI) and stem area index (SAI) and is calculated as

$$\varepsilon_v = 1 - e^{-(\mathrm{LAI}+\mathrm{SAI})}. \tag{1}$$

Using the Stefan-Boltzmann law, subcanopy longwave radiation is calculated as

$$LW_{sub} = (1-\varepsilon_v)\, LW_{atm} + \varepsilon_v\, \sigma\, T_{veg}^4 \tag{2}$$

with Stefan-Boltzmann constant $\sigma = 5.67 \cdot 10^{-8}\ \mathrm{W{\cdot}m^{-2}{\cdot}K^{-4}}$ and vegetation temperature T_{veg}. This vegetation temperature is calculated based on vegetation temperature from the previous time step and the change in vegetation temperature from the previous to the current time step as

$$T_{veg}^4 = \left(T_{veg}(t-1)\right)^4 + 4\ \left(T_{veg}(t-1)\right)^3\ \left(T_{veg}(t) - T_{veg}(t-1)\right). \tag{3}$$

Vegetation temperature in CLM4.5 is calculated based on an energy balance, net radiation minus turbulent heat fluxes. Radiative transfer of direct and diffuse shortwave radiation is calculated via a two-stream approximation (Sellers, 1985), and CLM4.5 considers a single reflection of shortwave radiation from the ground to the canopy. Net longwave radiation is calculated from vegetation temperature, atmospheric longwave radiation, and (ground) surface temperature and determined by vegetation emissivity and emissivity of the ground. Emissivity of the ground is a weighted sum of soil and snow emissivities (0.96 and 0.97, respectively). Calculation of turbulent heat fluxes in CLM4.5 is based on Monin-Obukhov similarity theory and described by Oleson et al. (2013).

2.2. SNOWPACK

Gouttevin et al. (2015) improved the canopy module within SNOWPACK from a one-layer big-leaf vegetation scheme by addition of biomass heat storage and partitioning of the vegetation canopy into two interacting layers, an upper layer and a lower layer associated with different vegetation parts (leaves and trunk, respectively). The radiation scheme for vegetation in SNOWPACK is displayed in Figure 1. Subcanopy longwave radiation is a combination of longwave radiation emitted by, and atmospheric longwave radiation passing through, the vegetation layers. Absorption factors determine the fractions of these components for each layer and are also used for shortwave radiation in contrast to the two-stream approximation used in CLM4.5. Absorption factor σ_f for longwave and diffuse shortwave radiation is calculated as a combination of absorption factors for both vegetation layers:

$$1 - \sigma_f = (1 - \sigma_{f,\mathrm{leaf}})\,(1 - \sigma_{f,\mathrm{trunk}}), \tag{4}$$

which are calculated as

$$\sigma_{f,\mathrm{leaf}} = 1 - e^{-k_{\mathrm{LAI}}\, f_{\mathrm{LAI}}\, \mathrm{LAI}} \tag{5}$$

and

$$\sigma_{f,\mathrm{trunk}} = 1 - e^{-k_{\mathrm{LAI}}\, (1-f_{\mathrm{LAI}})\, \mathrm{LAI}} \tag{6}$$

and adjusted for direct shortwave radiation using solar elevation angle. Absorption is spread across both vegetation layers depending on total LAI, that is, the sum of both layers, with f_{LAI} determining the fraction assigned to the upper (leaf) layer. Calculation of total absorption σ_f is similar to the calculation of vegetation emissivity ε_v in CLM4.5 but additionally comprises an extinction coefficient k_{LAI}, the value of which is typically between 0.4 and 0.8 (Gouttevin et al., 2015). The improved canopy module of SNOWPACK was calibrated at the subalpine site of Alptal, Switzerland, with parameters set to $f_{\mathrm{LAI}} = 0.5$ and $k_{\mathrm{LAI}} = 0.75$, and emissivities of both vegetation layers were set to 1 to suppress multiple reflections. Calculation of subcanopy longwave radiation is similar to equation (2), but absorption factors determine contributions of individual vegetation layers to LW_{veg}:

$$LW_{\mathrm{sub}} = (1 - \sigma_f)\, LW_{\mathrm{atm}} + (1 - \sigma_{f,\mathrm{trunk}})\, \sigma_{f,\mathrm{leaf}}\, \sigma\, T_{\mathrm{leaf}}^4 + \sigma_{f,\mathrm{trunk}}\, \sigma\, T_{\mathrm{trunk}}^4 \tag{7}$$

with vegetation temperatures of the respective layers T_{leaf} and T_{trunk} using the Stefan-Boltzmann equation. For the calibrated value of $f_{\mathrm{LAI}} = 0.5$, absorption factors of both layers are equal and the lower layer exhibits a higher impact on subcanopy longwave radiation than the upper layer.

Vegetation temperatures in SNOWPACK are calculated via energy balances for each layer. Net radiation is calculated from insolation, atmospheric longwave radiation, and surface temperature based on absorption factors, vegetation albedos, ground albedo, and ground emissivity and includes multiple reflections of shortwave radiation between canopy and ground. Turbulent fluxes are calculated using bulk formulations (Gouttevin et al., 2015). In contrast to CLM4.5 and the initial one-layer version, SNOWPACK additionally comprises heat storage and release by biomass. This biomass heat flux BM_i of vegetation layer i (leaf or trunk) is parameterized by a temperature change for time step Δt and heat mass of vegetation:

$$BM_i(t) = HM_i\, \frac{T_i(t) - T_i(t-1)}{\Delta t}. \tag{8}$$

Heat mass HM_i is calculated as

$$HM_{\mathrm{leaf}} = \mathrm{LAI}\, e_{\mathrm{leaf}}\, \rho_{\mathrm{biomass}}\, C_{p,\mathrm{biomass}} \tag{9}$$

and

$$HM_{\mathrm{trunk}} = 0.5\, B\, z_{\mathrm{can}}\, \rho_{\mathrm{biomass}}\, C_{p,\mathrm{biomass}}, \tag{10}$$

depending on biomass specific heat mass $C_{p,\mathrm{biomass}} = 2{,}800\ \mathrm{J{\cdot}kg^{-1}{\cdot}K^{-1}}$, biomass density $\rho_{\mathrm{biomass}} = 900\ \mathrm{kg/m^3}$, typical leaf thickness $e_{\mathrm{leaf}} = 0.001$ m, LAI, canopy height z_{can}, and dimensionless stand basal area B. Interaction between the two layers in SNOWPACK is included in (1) net shortwave radiation via shading of the lower layer by the upper layer and (2) net longwave radiation as a layer emits longwave radiation upward and downward impacting the respective layer above or below.

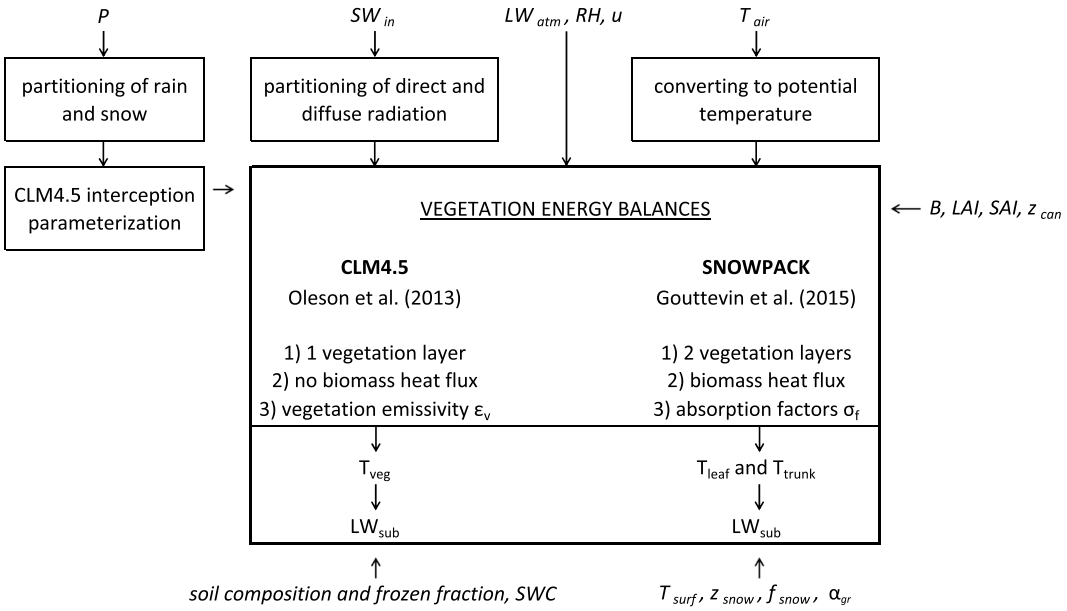

Figure 2. Schematic of Toy Model workflow. Symbols as in equations (1), (2), (7), and (10). *P* denotes precipitation. SW_{in} denotes incoming shortwave radiation. *RH* denotes relative humidity. The *u* denotes wind speed. T_{air} denotes air temperature. T_{surf} denotes surface temperature. The z_{snow} denotes snow depth. The f_{snow} denotes snow cover fraction. The α_{gr} denotes ground albedo. *SWC* denotes soil water content.

2.3. Toy Model Setup

Evaluation of subcanopy longwave radiation simulated by CLM4.5 and comparison to simulations by SNOWPACK necessitate the usage of forest stand-scale forcing and evaluation data for both models. Therefore, full energy balance calculations of both models were extracted from their respective original model codes to calculate vegetation temperatures, which were subsequently used to calculate subcanopy longwave radiation as outlined in equations (2) and (7). Workflow and required inputs are shown in Figure 2. The Toy Model allows for a direct comparison as vegetation is conceptualized as layers in both CLM4.5 and SNOWPACK and mostly characterized by the same parameters. CLM4.5 subdivides grid cells based on land units and plant functional types (PFTs); however, usage of stand-scale forcing effectively results in the simulation of a single grid cell solely covered by the specific PFT(s) of a forest stand, and consequently, the PFT coverage is 100%. This corresponds to the parameter throughfall fraction in SNOWPACK being set to 0, which is representative of complete canopy coverage and stand-scale averages.

The following assumptions and decisions were made to facilitate a direct comparison of CLM4.5 and SNOWPACK only focusing on differences in parameterizations of vegetation energy balances. Hourly time steps were used for both models and all forest stand sites. Interception of precipitation calculated by CLM4.5 was also used for SNOWPACK. Albedo, emissivity, and roughness length for soil and snow were prescribed as the same for both models, using values and parameterizations from CLM4.5. Ground albedo and emissivity were calculated as a combination of soil and snow values weighted by snow cover fraction. Calculation of snow albedo by the SNICAR module in CLM4.5 (Flanner & Zender, 2005) was replaced with a simple aging curve for forest floor albedo used in SNOWPACK, which only required a set value for snow albedo and age of snow on the ground. Fresh snow albedo was set to 0.8 in the Toy Model, which is slightly lower than the value of 0.84 used by Pomeroy et al. (1998). Insolation was assumed as visible since measurements of near-infrared shortwave radiation were not available and SNOWPACK does not distinguish between visible and near-infrared wavebands. A lapse rate-adjusted potential temperature, scaled from forcing height to surface, is used in CLM4.5, and this temperature was also used for SNOWPACK. Soil quantities were averaged vertically for CLM4.5 in lieu of consistent measurements of vertical profiles.

The effect of a biomass heat storage parameterization on subcanopy longwave radiation in CLM4.5 was tested, for which the parameterization used in SNOWPACK (equations (8)–(10)) was implemented in CLM4.5 (henceforth, CLM4.5-BM). As in SNOWPACK, biomass heat flux was added to turbulent heat fluxes resulting in a

Table 1
Characteristics of Forest Stand Sites

Characteristic	Abisko	Alptal[a]	Borden	Cherskiy	Seehornwald[b]	Sodankylä	Yakutsk
Latitude	68.4°N	47.1°N	44.3°N	68.7°N	46.8°N	67.4°N	62.3°N
Longitude	18.8°E	8.8°E	79.9°W	161.4°E	9.9°E	26.6°E	129.6°E
Altitude	388 m	1,220 m	222 m	39 m	1,640 m	179 m	220 m
Snowmelt season	2011	2004–2007	2013	2017	2008–2012	2012	1998
Evaluation start	11 Mar		2 Jan	30 Mar	1 Jan	10 Mar	14 Feb
Evaluation end	3 Apr		4 Apr	21 May		16 Apr	14 May
Evaluation days	9		77	51		37	87
Vegetation	birch	spruce	mixed	larch	spruce	pine	larch
PFT	BDBT	NEBT	BDTT, NETT	NDBT	NEBT	NEBT	NDBT
Tree height	3.5 m	25 m	22 m	5 m	25 m	18 m	18 m
Tree diameter	3.8 cm	100 cm	6.8 cm, 12.3 cm	1.7 cm	40 cm	11.6 cm	25.6 cm
Stand basal area (m^2/m^2)	0.0006	0.004	0.0011, 0.0036	0.0048	0.0166	0.002	0.004
SAI (m^2/m^2)	0.44	0.86	1.10, 0.48	0.67	1.2	0.25	1.71
LAI (m^2/m^2)	0	3.24	0.05, 1.93	0	3.9	0.89	0
PAI (m^2/m^2)	0.44	4.1	1.15, 2.41	0.67	5.1	1.14	1.71
Soil albedo	—	0.11	0.20	0.09	0.19	—	0.19
Clay	19%	24%	3%	19%	31%	12%	26%
Sand	54%	48%	71%	46%	52%	61%	41%
Organic matter	7%	7%	6%	12%	8%	25%	9%

Note. Evaluation periods start at 1:00 and end at 0:00 on the given day. Evaluation days differ from the length of evaluation periods due to quality control of measurements. Acronyms of PFTs denote Broadleaf Deciduous Boreal Trees (BDBTs), Needleleaf Deciduous Boreal Trees (NDBTs), Needleleaf Evergreen Boreal Trees (NEBTs), Broadleaf Deciduous Temperate Trees (BDTTs), and Needleleaf Evergreen Temperate Trees (NETTs). Soil albedo for Abisko and Sodankylä were not determined due to constant snow cover on the ground. Fractions of soil composition were taken from CLM4.5's 0.23° × 0.31° surface data set and averaged vertically. PFT = plant functional type; SAI = stem area index; LAI = leaf area index; PAI = plant area index.
[a]Evaluation periods at Alptal start on 1 January except for 2004 (24 January). Dates for end of evaluation period at Alptal are 12 March 2004, 14 March 2005, 19 March 2006, and 4 April 2007. Evaluation durations for Alptal are 41 days in 2004, 57 days in 2005, 73 days in 2006, and 85 days in 2007. [b]Dates for end of evaluation period at Seehornwald are 27 April 2008, 1 April 2009, 20 April 2010, 29 March 2011, and 26 April 2012. Evaluation durations for Seehornwald are 116 days in 2008, 90 days in 2009, 106 days in 2010, 83 days in 2011, and 116 days in 2012.

vegetation energy balance of net radiation minus turbulent heat fluxes minus biomass heat flux. Biomasses of needles (equation (9)) and trunks (equation (10)) were combined for the single vegetation layer in CLM4.5-BM.

3. Forcing and Evaluation Data

3.1. Description of Forest Stand Sites

The Toy Model was used to simulate subcanopy longwave radiation for seven forest stands, which span a wide range of vegetation types and structures as well as meteorological conditions. Site characteristics are shown in Table 1, including type, height, and density of vegetation. Measurements and approximations of forcing variables are listed in Table 2. Descriptions of approximations, used if no measurements were available, and sensitivity tests are given in supporting information (Text S1, Figures S1 to S7, and Tables S1 to S5). Measurements of subcanopy longwave radiation and stand characteristics at each site are described in the following.

3.1.1. Alptal, Switzerland

Descriptions of the forest stand are given by Rutter et al. (2009), Stähli et al. (2009), and Gouttevin et al. (2015), the latter of which used data from this site to test and calibrate SNOWPACK. Subcanopy longwave and shortwave radiation were measured by a moving radiometer on a rail of 10-m length, which covered one length of the rail every 10 min representing a spatial average for each hourly time step. Subcanopy longwave radiation measurements were checked for potential errors caused by snow cover on radiometers, and those time steps were excluded from analysis (description in supporting information). Studies give different LAI values for Alptal, mean stand LAI of 3.9 m^2/m^2 (Gouttevin et al., 2015) and total LAI of 4.2 m^2/m^2 (Rutter et al., 2009), while Stähli et al. (2009) give a range for LAI along the rail based on hemispherical photography. Total LAI includes woody parts and thus represents plant area index (PAI), indicating LAI values given by Stähli et al. (2009) and

Table 2
Measurement Locations, Measurement Methods, and Approximations of Forcing Variables

Forcing	Abisko	Alptal	Borden	Cherskiy	Seehornwald	Sodankylä	Yakutsk
LW_{atm}	open	tower	tower	tower	tower	open	tower
P	open	open	open	open	tower	open	open
RH	open	open	tower	tower	tower	tower	tower
SW_{in}	open	tower	tower	tower	tower	open	tower
T_{air}	open	tower	tower	tower	tower	tower	tower
u	open	tower	tower	open	tower	tower	tower
z_{snow}	open	forest, manual	assumption	assumption	open, scaled	open, scaled	assumption
LW_{sub}	4 radiometers	rail	single radiometer	single radiometer	rail	4 radiometers	residual
SWC	proxy (GWL)	proxy (GWL)	vertical profile	vertical profile	single depth	vertical profile	vertical profile
T_{soil}	vertical profile	single depth	vertical profile	vertical profile	single depth	vertical profile	vertical profile
f_{diff}	measured	ε_{sky}	ε_{sky}	ε_{sky}	potential insolation	measured	ε_{sky}
f_{snow}	constant	α_{surf}	α_{surf}	α_{surf}	α_{surf}	constant	top T_{soil}
$f_{rainfall}$	threshold (2 °C)	transition (0–1.5 °C)	threshold (2 °C)	threshold (2 °C)	transition (0–1.5 °C)	threshold (2 °C)	threshold (2 °C)
T_{surf}	T_{air} (0.5 m)	LWR	LWR	LWR	LWR	T_{air} (0.5 m)	measured

Note. Symbols as used in Figure 2. The ε_{sky} indicates effective emissivity of the sky (equation (11)) was used to approximate the fraction of diffuse shortwave radiation f_{diff}. GWL indicates that ground water level was used to approximate soil water content. LWR indicates outgoing longwave radiation was used to estimate surface temperature. Soil temperature T_{soil} was used to estimate fraction of frozen soil. Calculation of rainfall fraction $f_{rainfall}$ out of precipitation was based on either the transition algorithm given by Rutter et al. (2009) for Alptal or the threshold algorithm given by Essery et al. (2016) for Sodankylä.

Gouttevin et al. (2015) also represent PAI. An average of 4.1 m^2/m^2 along the rail was used as PAI; LAI and SAI were estimated using their respective fractions of PAI taken from Alptal's corresponding grid cell and PFT in the high-resolution surface data set of CLM4.5.

3.1.2. Seehornwald, Switzerland

Descriptions of the forest stand near Davos, Switzerland, are given by Webster et al. (2016b) and Zweifel et al. (2016). LAI was taken from Webster et al. (2016b), and SAI was calculated as for Alptal using the value from Seehornwald's corresponding grid cell and PFT. Stand basal area was calculated from tree diameter and tree density given online by the Swiss Long-Term Forest Ecosystem Research program. Subcanopy longwave and shortwave radiation were measured by the rail setup described for Alptal, which was moved to Seehornwald in 2007.

3.1.3. Sodankylä, Finland

Descriptions of the forest stand are given by Hancock et al. (2014) and Reid, Essery, et al. (2014), where it is listed as site C out of multiple sites at Sodankylä. Subcanopy longwave radiation was measured by four radiometers providing a spatial average for this study. Radiometers were checked and quality controlled on a daily basis. PAI was estimated from hemispheric photos for each radiometer location ranging from 1.09 to 1.22 m^2/m^2 and averaging 1.14 m^2/m^2. LAI and SAI were estimated as for Alptal using the value from Sodankylä's corresponding grid cell and PFT.

3.1.4. Cherskiy, Russia

Description of the forest stand near Cherskiy, Russia, is given by Alexander et al. (2012), where it is listed as stand 13. The forest stand differs in vegetation structure compared to previous sites, as trees are smaller and thinner (Table 1) but tree density is high (3.7 trees m^{-2}). A canopy top height of 5 m was used for this study instead of mean stand height of 3.4 m given by Alexander et al. (2012). LAI was set to 0 as vegetation was leafless throughout the evaluation period. SAI was estimated as the lateral surface area of conical trees based on tree height and tree diameter. Radiation measurements were quality controlled for snow cover on radiometers.

3.1.5. Abisko, Sweden

Descriptions of the forest stand are given by Reid, Essery, et al. (2014) and Reid, Spencer, et al. (2014), where it is listed as site C out of multiple sites at Abisko. Subcanopy longwave radiation was measured by four

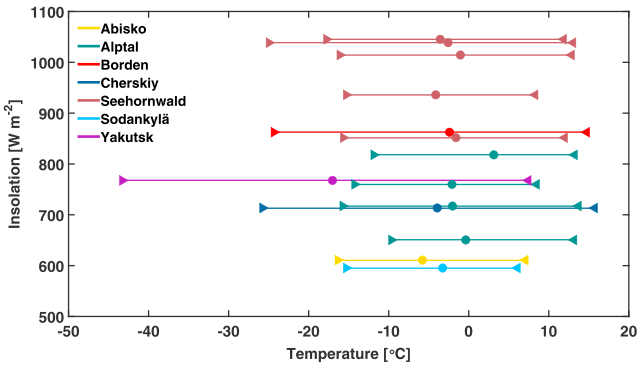

Figure 3. Comparison of air temperature (minimum, mean, and maximum) and maximum insolation over respective evaluation periods (see Table 1) for forest stand sites Abisko (yellow), Alptal (green, individual years), Borden (red), Cherskiy (dark blue), Seehornwald (maroon, individual years), Sodankylä (light blue), and Yakutsk (violet). Maximum insolation at Yakutsk is shown only for context, as evaluation was limited to nighttime.

radiometers, providing a spatial average for this study, and quality controlled by Reid, Essery, et al. (2014). PAI was estimated from hemispheric photos for each radiometer location ranging from 0.14 to 0.70 m^2/m^2 and averaging 0.44 m^2/m^2. LAI was set to 0 and SAI set to PAI as the forest consists of birch trees that were leafless throughout the evaluation period.

3.1.6. Yakutsk, Russia

Description of the forest stand north of Yakutsk, Russia, is given by Ohta et al. (2001) stating trees were still leafless after snowmelt with an SAI of 1.71 m^2/m^2, so that LAI was set to 0. Mean tree diameter was estimated corresponding to mean stand height based on diameters and heights for four trees used for sap flow measurements (Ohta et al., 2001).

Subcanopy measurements included incoming and outgoing shortwave radiation, net all-wave radiation, and surface temperatures, and subcanopy longwave radiation was calculated as a residual. However, incoming shortwave radiation below the canopy displayed large fluctuations compared to outgoing shortwave radiation resulting in occasional negative net shortwave radiation, which was potentially caused by the usage of a single radiometer. Consequently, only nighttime subcanopy longwave radiation was used for this study.

3.1.7. Borden, Canada

Descriptions of forest stand and instrumentation are given by Teklemariam et al. (2009) and Froelich et al. (2015), respectively. The forest stand consists of deciduous broadleaf and evergreen needleleaf trees, so that two PFTs were used for CLM4.5 simulations. Fractions of PFTs were based on the most recent tree survey described by Teklemariam et al. (2009), yielding 18.7% for evergreen needleeleaf trees and 81.3% for deciduous broadleaf trees, and used to weight subcanopy longwave radiation calculated separately for each PFT. Temperate instead of boreal PFTs were used as the Borden forest is located in the southern part of the North American deciduous-boreal forest ecotone. Tree diameter and stand basal area for each PFT were estimated based on tree diameters given by Neumann et al. (1989) and the tree survey described by Teklemariam et al. (2009). Post-leaf out LAI for the forest stand is given as 4.6 m^2/m^2 by Croft et al. (2015). Pre-leaf out and post-leaf out stand PAI were measured as 1.36 and 5.6 m^2/m^2, respectively. LAI and PAI measurements, LAI-to-SAI fractions from CLM4.5's high-resolution surface data set for corresponding PFTs and grid cell, and PFT fractions were used to calculate LAI and SAI values for both PFTs. Subcanopy radiation measurements were quality controlled for snow cover on radiometers.

3.2. Site Comparison

This study uses data from seven forest stands, of which three consist of evergreen needleleaf trees, three consist of deciduous trees, and one is a mixed forest of both evergreen and deciduous trees. The current version of SNOWPACK is only suited for evergreen sites as it was developed for alpine forests (Gouttevin et al., 2015), so that its usage was limited to Alptal, Seehornwald, and Sodankylä. The start of the evaluation period at each site was determined by data availability except for Alptal (2005-2007) and Seehornwald, for which evaluation start was set to 1 January. End of evaluation period was determined by data availability for Abisko and Sodankylä. For Alptal, Borden, Cherskiy, Seehornwald, and Yakutsk, end of evaluation period was determined by meltout, which was estimated from surface albedo measurements.

Air temperatures are similar across most sites (Figure 3), the exception being Yakutsk for which evaluation started 4 to 6 weeks earlier than for the other high-latitude sites Abisko, Cherskiy, and Sodankylä. Maximum insolation varies across sites; Borden and Seehornwald display larger insolation maxima due to latitude and duration of evaluation period. A means of categorizing meteorological conditions is effective emissivity of the sky, ε_{sky}, which is calculated as

$$\varepsilon_{sky} = \frac{LW_{atm}}{\sigma\, T_{air}^4} \tag{11}$$

and varies greatly based on cloudiness. For clear skies, effective temperature of the atmosphere decreases reducing the amount of atmospheric longwave radiation reaching vegetation and ground. Conversely, effective temperature for overcast conditions is similar to or higher than actual air temperature resulting in ε_{sky} close to or larger than 1. Effective emissivity of the sky is a dimensionless quantity and thus suitable to compare

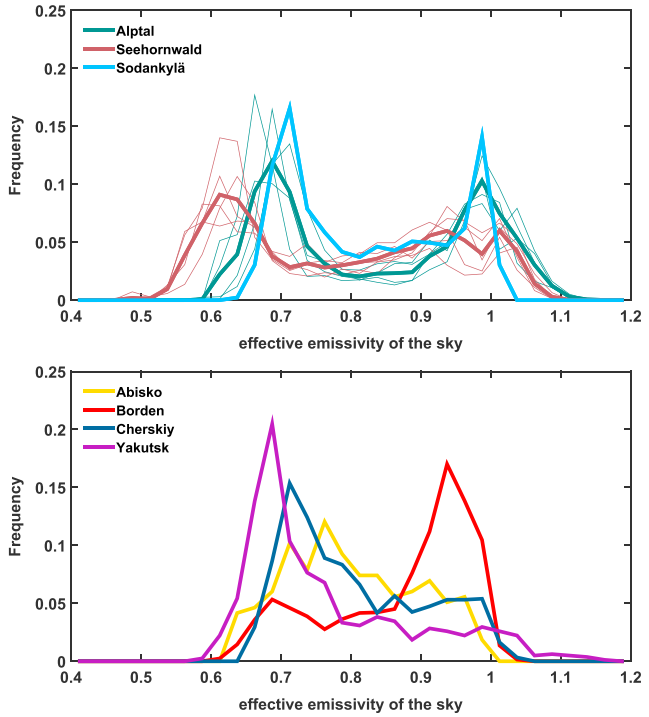

Figure 4. Probability Density Functions of effective emissivities of the sky over respective evaluation periods (see Table 1) for evergreen (top) and deciduous (bottom) Toy Model sites Abisko (yellow), Alptal (green), Borden (red), Cherskiy (dark blue), Seehornwald (maroon), Sodankylä (light blue), and Yakutsk (violet). Multiple lines for Alptal and Seehornwald display total (bold line) and individual years (thin lines).

different locations, and Probability Density Functions (PDFs) of ε_{sky} are shown in Figure 4. Abisko, Cherskiy, and Yakutsk exhibit one clear peak at low emissivity values indicating mostly clear-sky conditions, while there is one peak at high emissivity values for Borden indicating mostly overcast conditions. Alptal, Sodankylä, and, to a lesser degree, Seehornwald exhibit two peaks, one at each end of the spectrum, indicating varying degrees of cloudiness.

4. Results

4.1. Comparison of Subcanopy Longwave Radiation Simulated by CLM4.5 and SNOWPACK With Observations

Simulated and observed subcanopy longwave radiation for evergreen sites are compared in Figure 5. Ranges of observations and simulations differ between sites as a consequence of differences in vegetation density (Table 1) and meteorological forcing (Figure 3). Simulations by CLM4.5 display a larger spread than simulations by SNOWPACK for both Alptal and Seehornwald, resulting in root-mean-square error (RMSE) values about twice as high as for SNOWPACK. For Sodankylä, spread in subcanopy longwave radiation simulated by CLM4.5 is smaller than for Alptal and Seehornwald, with RMSE being smaller by about 50%, and similar to the spread simulated by SNOWPACK. Simulations by CLM4.5 exhibit a substantially negative mean bias (MB) for Alptal, in contrast to simulations by SNOWPACK, while MB values are close to 0 for Seehornwald and Sodankylä. For SNOWPACK, MB is close to 0 for Alptal but substantially larger in absolute terms for Seehornwald and Sodankylä. RMSE values are also higher for Seehornwald and Sodankylä compared to Alptal, for which SNOWPACK was calibrated; however, the spread in subcanopy longwave radiation simulated by SNOWPACK is similar for all evergreen sites. Both RMSE and MB can be improved for SNOWPACK via calibration, mainly by increasing (decreasing) extinction coefficient k_{LAI} for lower (higher) vegetation density (supporting information, Figures S9 and S10).

4.2. Simulation of Longwave Enhancement by CLM4.5

Relative errors of subcanopy longwave radiation simulated by CLM4.5 are shown in Figure 6. Evergreen sites and Cherskiy display the same triangular pattern; errors increase in absolute terms for lower values of ε_{sky} with overestimation during daytime and underestimation during nighttime. The range of errors is higher for Alptal than for Sodankylä and Cherskiy when comparing the range of ε_{sky} and insolation present at Sodankylä and Cherskiy. Simulations for Seehornwald display a higher range of errors than for Alptal when comparing similar meteorological conditions and larger maximum overestimation due to later meltout leading to higher

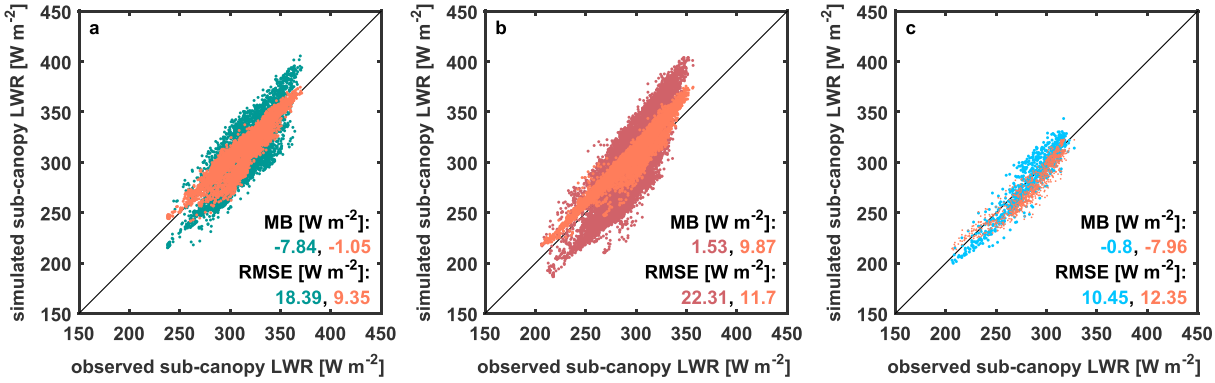

Figure 5. Comparison of observed and simulated subcanopy longwave radiation for (a) Alptal, (b) Seehornwald, and (c) Sodankylä. SNOWPACK simulations are shown in orange, while CLM4.5 simulations are shown in green (Alptal), maroon (Seehownwald), and light blue (Sodanklya). Mean bias (MB) and root-mean-square error (RMSE) values are given in Table 3 for comparison with deciduous forest stands. LWR = longwave radiation.

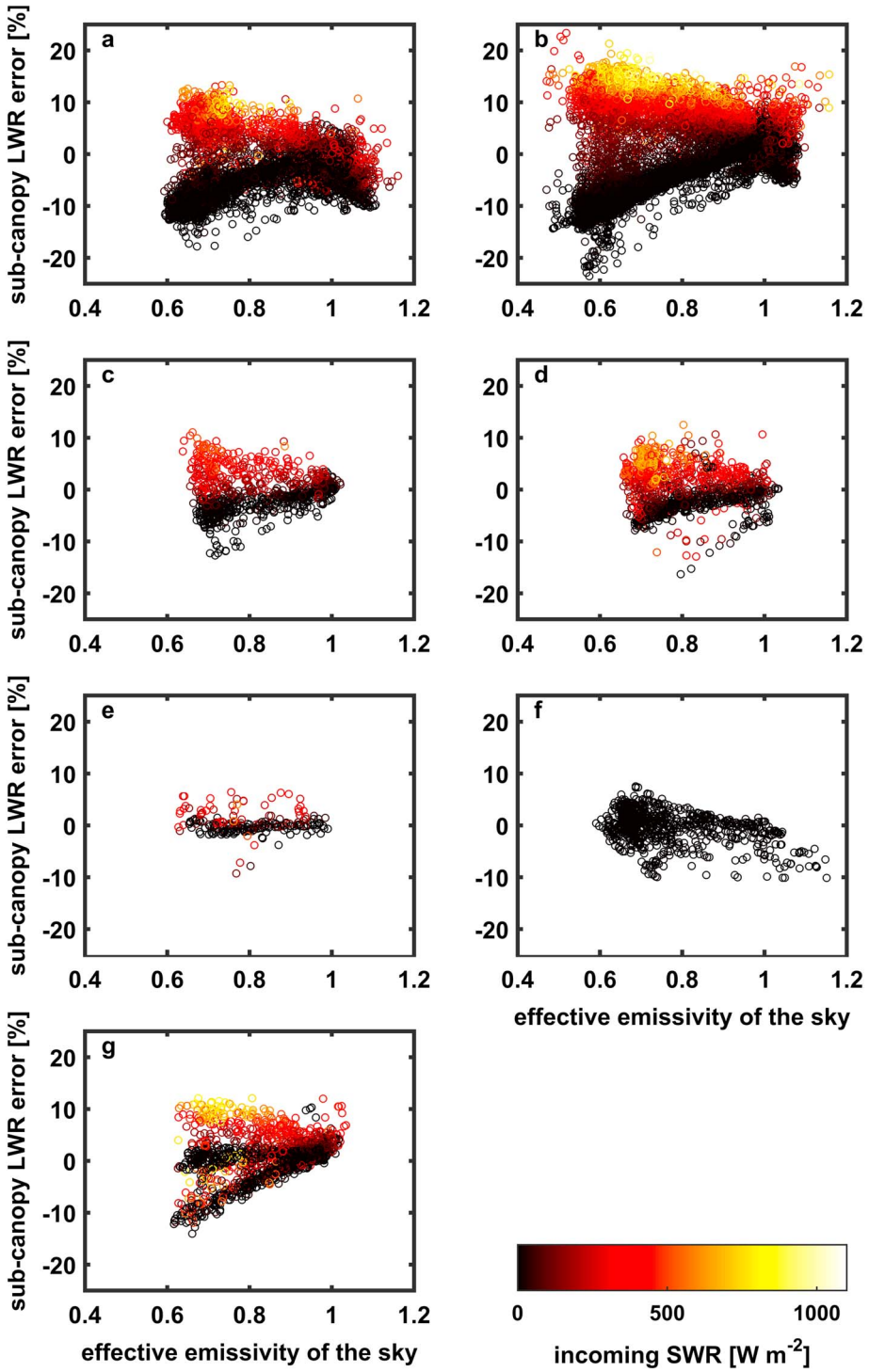

Figure 6. Subcanopy longwave radiation errors simulated by CLM4.5 relative to observations as a function of effective emissivity of the sky (abscissa) and insolation (color) for (a) Alptal, (b) Seehornwald, (c) Sodankylä, (d) Cherskiy, (e) Abisko, (f) Yakutsk, and (g) Borden. Values for Yakutsk are shown only for nighttime. Errors are negative for underestimation by CLM4.5 and positive for overestimation by CLM4.5. LWR = longwave radiation; SWR = shortwave radiation.

Table 3
Root-Mean-Square Error (RMSE) and Mean Bias (MB) for Subcanopy Longwave Radiation Simulated by CLM4.5 Before and After (CLM4.5-BM) Including a Biomass Heat Storage Parameterization

	RMSE (W/m^2)			MB (W/m^2)		
Site	CLM4.5	CLM4.5-BM	SNOWPACK	CLM4.5	CLM4.5-BM	SNOWPACK
Abisko	5.65	5.47	—	0.70	0.64	—
Alptal	18.39	14.72	9.35	−7.84	−5.63	−1.05
Borden	11.27	10.79	—	3.37	4.55	—
Cherskiy	11.30	10.55	—	0.70	0.86	—
Seehornwald	22.31	15.75	11.70	1.53	10.44	9.87
Sodankylä	10.45	9.20	12.35	−0.80	−0.08	−7.96
Yakutsk	6.92[a]	8.45[a]	—	−0.37[a]	1.46[a]	—

Note. Values for Alptal and Seehornwald were calculated for all years combined. SNOWPACK was only used for evergreen sites.
[a]Values for Yakutsk were calculated only for nighttime.

maximum insolation. For ε_{sky} reaching values larger than 1, which occurs regularly for Alptal and Seehornwald in contrast to Sodankylä and Cherskiy, nighttime underestimation increases in absolute terms for higher ε_{sky}. For Abisko, relative errors decrease slightly for clearer skies during nighttime, resembling the pattern seen for previous sites, but there is no clear pattern in daytime errors. Relative errors for nighttime at Yakutsk contrast those for previous sites, with spread around 0 increasing for clearer skies. For Borden, the range of errors is similar to Alptal, although maximum insolation is higher. In addition, there are nighttime simulation errors close to 0 for the whole range of ε_{sky} and occasional daytime underestimations. RMSE values in Table 3 display a contrast between dense vegetation at Alptal and Seehornwald (18 and 22 W/m^2, respectively), low-to-medium density vegetation with values between 10 and 12 W/m^2 (Borden, Cherskiy, and Sodankylä), and sparse vegetation at Abisko (6 W/m^2). Both RMSE and MB exhibit sensitivity to variations in PAI (supporting information Tables S6 and S7). Minimum RMSE can be found varying measured PAI by ±20% except for Alptal and Seehornwald, for which decreasing vegetation density results in smaller RMSE values. Increasing (decreasing) measured PAI results in MB increasing (decreasing) for all sites except Alptal and Seehornwald, for which sensitivity to PAI is substantially smaller and shows decreasing MB for increasing vegetation density.

The patterns seen for subcanopy longwave radiation translate to longwave enhancement displaying nighttime underestimation and daytime overestimation (Figure 7). Both longwave enhancement and ε_{sky} depend on atmospheric longwave radiation. For clear skies, atmospheric longwave radiation decreases resulting in decreasing ε_{sky} and increasing longwave enhancement during both daytime and nighttime, while insolation is higher during clear-sky days increasing vegetation temperatures. Therefore, increasing absolute errors of subcanopy longwave radiation for clearer skies result in increasing absolute errors for higher longwave enhancement. Alptal, Seehornwald, Sodankylä, Cherskiy, and Borden display this pattern, however, neither Abisko nor Yakutsk do. Ranges of longwave enhancement differ substantially between sites. At Seehornwald, longwave enhancement values of more than 1.9 and less than 0.9 have been observed. At Alptal, Borden, and Yakutsk, longwave enhancement values of up to 1.6 have been observed. Ranges of observed longwave enhancement values are smaller and similar for Cherskiy and Sodankylä and distinctly smaller for Abisko.

The impact of vegetation density on longwave enhancement can be seen in Figure 8. PDFs of observed longwave enhancement reveal a bimodal distribution for every site except Abisko and Borden. The first peak occurs for longwave enhancement values around 1 indicating little to no effect of the vegetation, which coincides with high ε_{sky} (overcast conditions). This peak is generally well represented by CLM4.5 except for Cherskiy. The second peak of observed longwave enhancement occurs for varying longwave enhancement values across sites and changes in accordance with vegetation density and ε_{sky}. Higher vegetation density and lower ε_{sky} result in higher longwave enhancement. For the dense forests at Alptal and Seehornwald, the second peak is clearly distinguishable from the first. Peaks are closer for Sodankylä and overlap for Cherskiy and Yakutsk, while there is no distinction for Abisko. The frequency of longwave enhancement is in accordance with the frequency of ε_{sky} (Figure 4), so that the second peak of longwave enhancement is more dominant at Cherskiy and Yakutsk while there is no clear second peak for Borden. Overestimations and underestimations

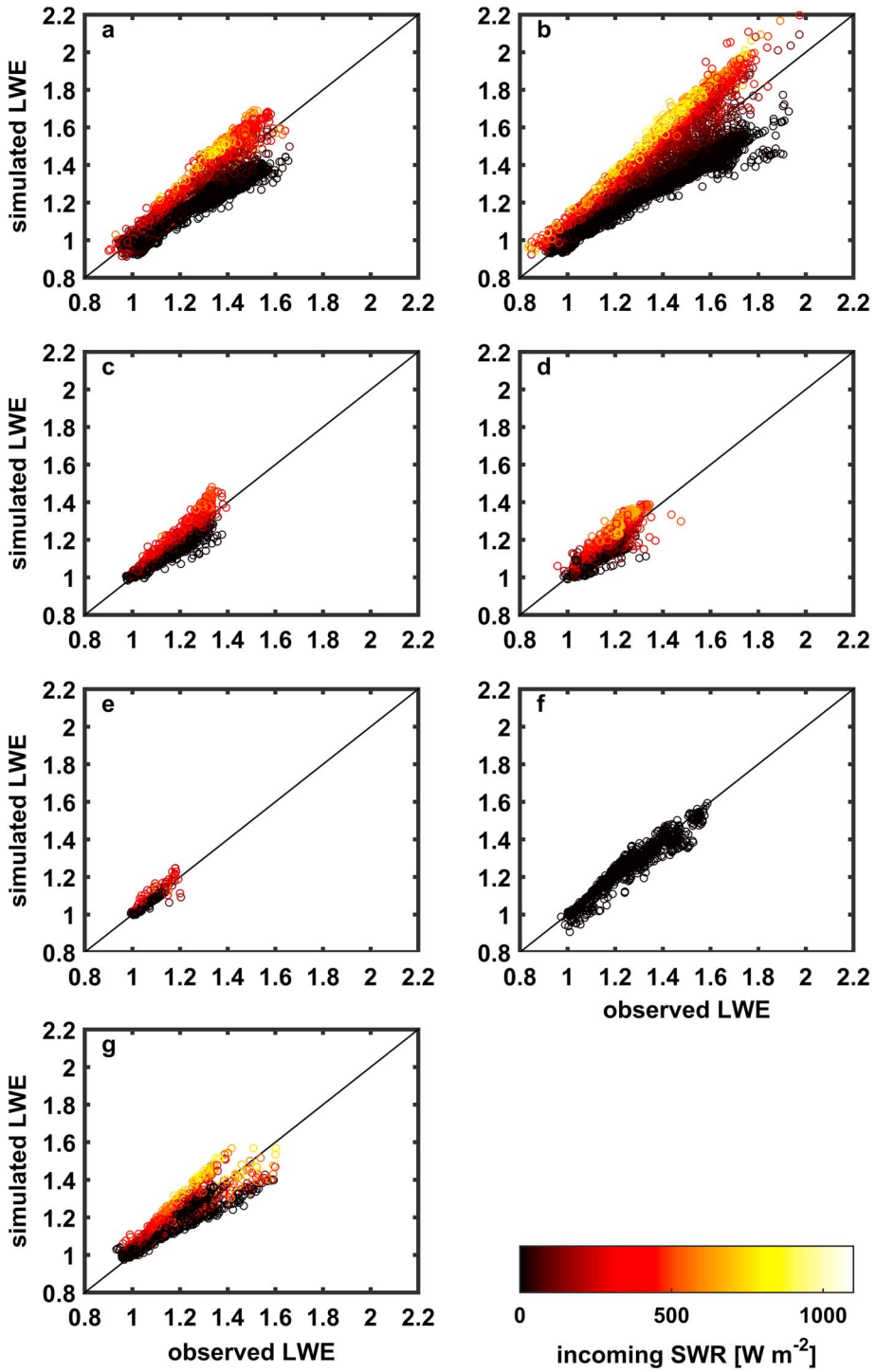

Figure 7. Comparison of observed longwave enhancement and longwave enhancement simulated by CLM4.5 as a function of insolation for (a) Alptal, (b) Seehornwald, (c) Sodankylä, (d) Cherskiy), (e) Abisko, (f) Yakutsk, and (g) Borden. Values for Yakutsk are shown only for nighttime. LWE = longwave enhancement; SWR = shortwave radiation.

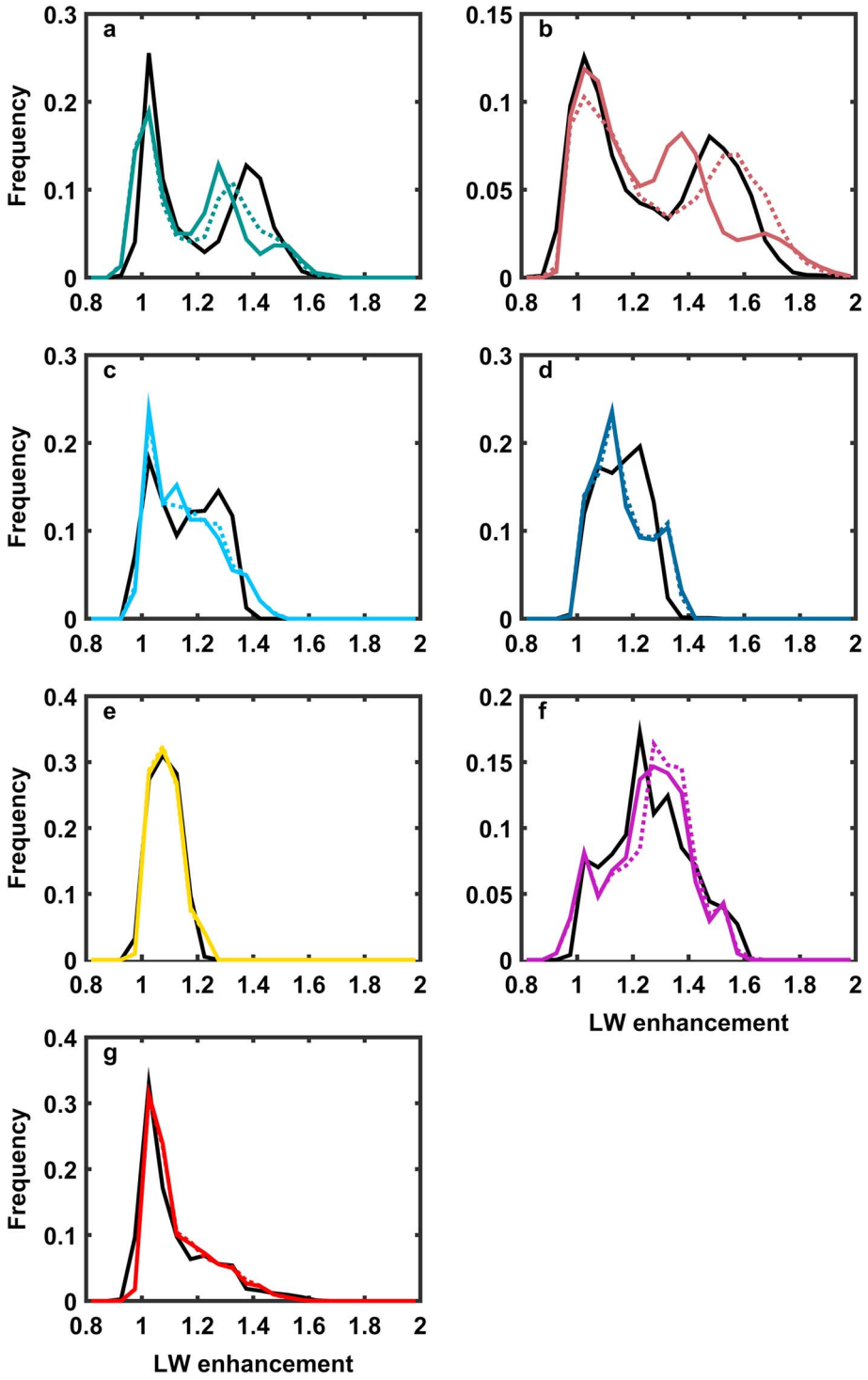

Figure 8. Probability Density Functions of longwave enhancement for observations (black), CLM4.5 (colored, solid), and CLM4.5 including biomass heat storage (colored, dashed) for (a) Alptal (green), (b) Seehornwald (maroon), (c) Sodankylä (light blue), (d) Cherskiy (dark blue), (e) Abisko (yellow), (f) Yakutsk (violet), and (g) Borden (red). Probability Density Function for Yakutsk was calculated from nighttime values. LW = longwave.

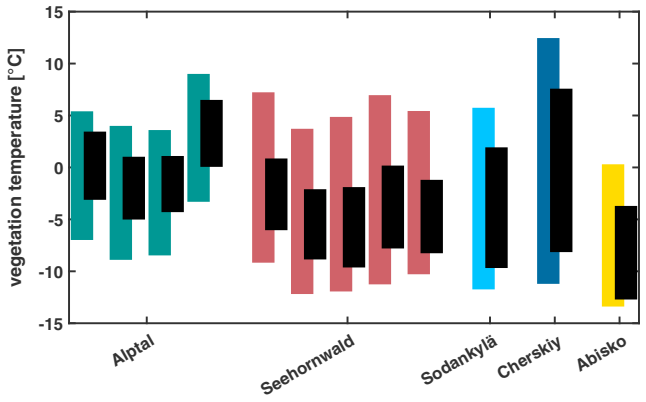

Figure 9. Comparison of average diurnal ranges of vegetation temperature calculated from observed subcanopy longwave radiation (black) and subcanopy longwave radiation simulated by CLM4.5 without biomass heat storage (colored) for Alptal (green, individual years), Seehornwald (maroon, individual years), Sodankylä (light blue), Cherskiy (dark blue), and Abisko (yellow). Borden is excluded from this analysis as the forest stand consists of multiple plant functional types and uncertainty in fractions of plant functional types affects the calculation of vegetation emissivities. Yakutsk is excluded as only nighttime values are used for this site.

by CLM4.5 found in Figures 6 and 7 can be seen for PDFs resulting in a separation of the second peak, which is more evident for the dense forests at Alptal and Seehornwald. For Sodankylä, CLM4.5 simulates no clear second peak, while the first and split-up second peak overlap for Cherskiy due to low vegetation density. For Abisko and Borden, CLM4.5 simulates the PDF of longwave enhancement well. Variation in PAI around measured values shows little to no impact on PDFs of longwave enhancement, and CLM4.5 consistently simulates a split second peak (supporting information, Figure S8).

As a test for potential improvement of CLM4.5, SNOWPACK's biomass heat storage parameterization has been included and resulting PDFs of longwave enhancement are shown as dashed lines in Figure 8. Inclusion of biomass heat storage displays little to no impact for Abisko, Borden, Cherskiy, Sodankylä, and Yakutsk due to small volumes of biomass. A clear impact on underestimation of the second peak can be seen for Alptal and Seehornwald and less so for Sodankylä, while there is little impact on overestimation. Consequently, inclusion of biomass heat storage has a net positive effect on simulated subcanopy longwave radiation, which can be seen in increasing MB values except for the sparsest vegetation at Abisko (Table 3). However, RMSE values are reduced by including biomass heat storage for all sites except Yakutsk.

4.3. Influence of Vegetation Density on Simulation Error

As seen in Figure 6 and Table 3, errors in subcanopy longwave radiation simulated by CLM4.5 are smaller for sparsely vegetated sites compared to densely vegetated sites. Observations of atmospheric longwave radiation are used in equation (2) leaving two potential sources of simulation errors, vegetation temperature T_{veg} and vegetation emissivity ε_v. Schematically, equal absolute errors in vegetation temperature result in smaller errors in subcanopy longwave radiation for sparse compared to dense vegetation due to the weighting by vegetation emissivity. Vegetation temperatures simulated by CLM4.5 (without biomass heat storage) and inferred from observed subcanopy longwave radiation are compared to examine differences in errors solely caused by simulated vegetation temperatures (Figure 9). Vegetation temperatures were inferred from observations by inverting equation (2) and using vegetation emissivity calculated by CLM4.5 (equation (1)).

Observations indicate similar average diurnal ranges of vegetation temperatures for the dense vegetation at Alptal and Seehornwald. Vegetation temperatures are lower on average at Seehornwald, likely caused by differences in evaluation periods and higher elevation of Seehornwald resulting in lower air temperatures (see Table 1 and Figure 3). Interannual variability is higher for Alptal than for Seehornwald, which is tied to differences in evaluation periods at Alptal (Table 1). Observations for Sodankylä and Cherskiy indicate higher average diurnal ranges of vegetation temperatures for sparser vegetation. Different ranges of vegetation temperatures between Sodankylä and Cherskiy are likely caused by differences in air temperatures, insolation, and ε_{sky} (Figures 3 and 4). Ranges of vegetation temperatures at Abisko are small compared to all other sites, however, evaluation period is substantially shorter at Abisko (Table 1). CLM4.5 overestimates average diurnal ranges of vegetation temperatures, extending both above and below observations. Average diurnal ranges of simulated vegetation temperatures are similar for Seehornwald and Sodankylä and slightly smaller for Alptal. As observations indicate a larger average diurnal range for Sodankylä than for the densely vegetated sites at Alptal and Seehornwald, simulated vegetation temperatures are closer to those inferred from observations for Sodankylä compared to Alptal and Seehornwald, which is also found for the deciduous, sparser vegetation at Abisko and Cherskiy.

5. Discussion

Magnitude and range of longwave enhancement vary across forest stands used for this study and depend on meteorological conditions as well as vegetation density and structure. Except for Abisko (small, sparse vegetation) and Borden (primarily overcast conditions), a substantial impact of vegetation on longwave radiation can be seen (Figure 8). This is especially true for evergreen forests, which are the predominant vegetation type of boreal forests. Coincidentally, all three evergreen sites feature a bimodal distribution of ε_{sky}, indicating no

domination of clear-sky or overcast conditions. At Seehornwald, which featured both the highest vegetation density and lowest ϵ_{sky}, observed hourly longwave enhancement values reached up to 2, that is, doubling of subcanopy compared to atmospheric longwave radiation, and observed hourly longwave enhancement values reached up to 1.6 even at the dense but (predominantly) deciduous forests near Borden and Yakutsk. These magnitudes indicate that longwave enhancement represents a substantial contribution to the surface energy balance below the canopy.

CLM4.5 overestimates subcanopy longwave radiation during the day and underestimates subcanopy longwave radiation at night, with larger errors occurring under clear-sky conditions. As the magnitude of longwave enhancement increases for clearer skies, CLM4.5 displays larger errors for higher longwave enhancement values. The range of overestimation and underestimation varies between sites as the contribution from vegetation depends on vegetation density. Higher vegetation density results in a higher fraction of subcanopy longwave radiation being attributed to vegetation, and consequently, simulation errors are more emphasized for dense compared to sparse vegetation. This results in RMSE and MB values for subcanopy longwave radiation being sensitive to changes in vegetation density; however, the systematic deficiency in simulated longwave enhancement (Figure 8) persists independent of potential uncertainty in vegetation density. Furthermore, vegetation temperatures indicate an impact of vegetation density on the response of vegetation to meteorological conditions, which CLM4.5 fails to capture contributing to simulation errors differing between sites (Figure 9). Including a term that accounts for heat stored in vegetation biomass results in a net increase of subcanopy longwave radiation, except for Abisko where vegetation is sparse and small, as this parameterization mostly affects vegetation temperatures during afternoon and evening by allowing the vegetation to remain warmer for longer. Consequently, there is little impact on the diurnal range of subcanopy longwave radiation; however, net overestimations are enhanced (see Table 3).

Although SNOWPACK exhibits less skill for Seehornwald and Sodankylä compared to Alptal, for which it was calibrated, simulated subcanopy longwave radiation consistently displays a small spread, which is substantially smaller than the spread simulated by CLM4.5 for the dense forests at Alptal and Seehornwald. This suggests a consistent impact of a two-layer vegetation, which affects vegetation temperatures and subsequently subcanopy longwave radiation both during daytime, by shading the lower layer, and during nighttime, by sheltering the lower layer from radiative cooling. However, this general dampening of temperature variations in the lower vegetation layer contrasts with findings of higher variability of trunk temperatures compared to needle temperatures due to insolation (Pomeroy et al., 2009), further highlighting the role and importance of vegetation density. SNOWPACK was calibrated by Gouttevin et al. (2015) using Alptal data and not adjusted for this study. Consequently, MBs are substantially larger in absolute terms for Seehornwald and Sodankylä, which feature varying vegetation density. Higher vegetation density at Seehornwald results in net overestimation, while lower vegetation density at Sodankylä results in net underestimation. Calibration results in substantial improvement of simulated subcanopy longwave radiation, which is mostly due to adjusting extinction of radiation (equations (5) and (6)) in accordance with vegetation density. Improvements to SNOWPACK by Gouttevin et al. (2015) and this study focused mainly on the impact of radiation. However, Bonan et al. (2017) found turbulence parameterizations having a substantial impact on, among other variables, radiative temperature and reduced overestimation of diurnal ranges by implementing a roughness sublayer and subdividing the vegetation layer.

Systematic overestimations and underestimations of subcanopy longwave radiation simulated by CLM4.5 across sites and vegetation types suggest that it may be possible to develop a correction to the parameterization of subcanopy longwave radiation that depends on meteorological conditions (Figure 6). Improvements of SNOWPACK have shown that a two-layer canopy vegetation can dampen overestimated diurnal variations leading to asymmetric above-canopy and subcanopy longwave radiation (Gouttevin et al., 2015). However, MBs are small compared to RMSE values across all sites (Table 3), apart from Seehornwald after including biomass heat storage, and simple scaling of diurnal cycles is likely to have little impact on MBs. Moreover, MBs vary between sites and depend on evaluation periods, and sensitivity studies indicate forcing choices can turn net overestimations into net underestimations and vice versa. Consequently, the impact of simulation errors in subcanopy longwave radiation on snowmelt in global simulations is uncertain and likely features substantial spatial variations. Implementation of biomass heat storage results in more realistic diurnal cycles of subcanopy longwave radiation; however, the impact on MBs is consistently positive increasing net overestimations. Generally, the single most important parameter for each vegetation type is vegetation density indicating that its representation in climate models is crucial, as it determines the contribution from

vegetation to subcanopy longwave radiation, thereby scaling simulation errors, and exhibits an impact on the response of vegetation to meteorological forcing.

6. Conclusion

This study created a model framework to facilitate the simulation of subcanopy longwave radiation by CLM4.5 and SNOWPACK, a snow cover model with a more complex canopy representation, under equal conditions using forcing data from several boreal and montane forest stands with varying vegetation density and structure. Simulations by CLM4.5 display an overestimated diurnal range of subcanopy longwave radiation and consequently an overestimated diurnal range in longwave enhancement by forest vegetation. Simulation errors for both of these quantities depend on vegetation density and meteorological conditions. Amplitudes of diurnal ranges for subcanopy longwave radiation and longwave enhancement increase with decreasing effective emissivity of the sky, implying overestimated absorption of insolation and overestimated radiative cooling at night. In contrast, SNOWPACK featuring a two-layer vegetation canopy simulates smaller ranges of subcanopy longwave radiation. Vegetation density determines the contribution from vegetation to subcanopy longwave radiation thereby scaling simulation errors. Inclusion of a parameterization for biomass heat storage, guided by SNOWPACK, improves simulation of subcanopy longwave radiation and longwave enhancement by CLM4.5 but does not substantially reduce diurnal ranges. This effect on subcanopy longwave radiation is similar to the recent model development of SNOWPACK (Gouttevin et al., 2015), in terms of both reduced RMSE and persistence of the overestimated diurnal range. The latter was corrected in SNOWPACK by partitioning the vegetation into two layers, which may provide guidance for further improvements of CLM4.5.

Acknowledgments
This research was supported by the Canadian Sea Ice and Snow Evolution (CanSISE) Network, which is funded by the Natural Science and Engineering Research Council of Canada's Climate Change and Atmospheric Research program. Funding was also provided by the U.S. National Science Foundation grant PLR-1417745 and The Picker Interdisciplinary Science Institute at Colgate University through Mike Loranty. The code of the Toy Model to run and analyze simulations and create figures used in this study is available on GitHub at https://github.com/mtodt/2018_ToyModel. CLM4.5 code was obtained from https://svn-ccsm-release.cgd.ucar.edu/model_versions/cesm1_2_0/models/lnd/clm/src/clm4_5/. The SNOWPACK model code was obtained from https://models.slf.ch/p/snowpack/. Forcing data for Alptal, Borden, and Seehornwald are available on GitHub at https://github.com/mtodt/2018_ToyModel. Ground water level measurements at Alptal were provided by Patrick Schleppi at the Swiss Federal Institute for Forest, Snow and Landscape Research WSL. Site characteristics of Seehornwald are given in the Long-Term Forest Ecosystem Research (LWF) program's site overview at https://www.wsl.ch/en/forest/forest-development-and--monitoring/long-term-forest--ecosystem-research-lwf/sites.html, where it is listed as Davos. Forcing data for Cherskiy can be accessed from the Arctic Data Center at https://arcticdata.io/catalog/#view/doi:10.18739/A2BG2H890, and measurements taken at the airport of Cherskiy are available on GitHub at https://github.com/mtodt/2018_ToyModel. Data from Abisko and Sodankylä were generated from the UK Natural Environment Research Council (NERC) grant NE/H008187/1 and can be accessed from the British Atmospheric Data Centre at http://catalogue.ceda.ac.uk/uuid/9c8c86ed78ae4836a336d45cbb6a757c for Sodankylä and http://catalogue.ceda.ac.uk/uuid/6947880b98d32e249a8638ebe768efd2 for Abisko. Additional measurements of meteorological and soil forcing data at Abisko were provided by the Swedish Polar Research Secretariat, and ground water level measurements are available online from the Geological Survey of Sweden. Yakutsk data are available online at http://www.jamstec.go.jp/iorgc/hcorp/data/database/cdc/siberia/sub4.html, where the site is listed as Larch Forest of Spasskaya Pad. We want to thank Takeshi Ohta at Nagoya University for his support using Yakutsk data. We would like to thank three anonymous reviewers whose helpful comments improved this paper.

References

Alexander, H., Mack, M., Goetz, S., Loranty, M., Beck, P., Earl, K., et al. (2012). Carbon accumulation patterns during post-fire succession in Cajander Larch (*Larix cajanderi*) forest of Siberia. *Ecosystems*, *15*(7), 1065–1082. https://doi.org/10.1007/s10021-012-9567-6

Bonan, G., Patton, E., Harman, I., Oleson, K., Finnigan, J., Lu, Y., & Burakowski, E. (2017). Modeling canopy-induced turbulence in the Earth system: A unified parameterization of turbulent exchange within plant canopies and the roughness sublayer (CLM-ml v0). *Geoscientific Model Development Discussions*, *2017*, 1–80. https://doi.org/10.5194/gmd-2017-261

Brutel-Vuilmet, C., Ménégoz, M., & Krinner, G. (2013). An analysis of present and future seasonal Northern Hemisphere land snow cover simulated by CMIP5 coupled climate models. *The Cryosphere*, *7*, 67–80. https://doi.org/10.5194/tc-7-67-2013

Croft, H., Chen, J., Froelich, N., Chen, B., & Staebler, R. (2015). Seasonal controls of canopy chlorophyll content on forest carbon uptake: Implications for GPP modeling. *Journal of Geophysical Research: Biogeosciences*, *120*, 1576–1586. https://doi.org/10.1002/2015JG002980

Derksen, C., & Brown, R. (2012). Spring snow cover extent reductions in the 2008–2012 period exceeding climate model projections. *Geophysical Research Letters*, *39*, L19504. https://doi.org/10.1029/2012GL053387

Ellis, C. R., Pomeroy, J. W., Brown, T., & MacDonald, J. (2010). Simulation of snow accumulation and melt in needleleaf forest environments. *Hydrology and Earth System Sciences*, *14*, 925–940. https://doi.org/10.5194/hess-14-925-2010

Essery, R. (2013). Large-scale simulations of snow albedo masking by forests. *Geophysical Research Letters*, *40*, 5521–5525. https://doi.org/10.1002/grl.51008

Essery, R., Kontu, A., Lemmetyinen, J., Dumont, M., & Ménard, C. (2016). A 7-year dataset for driving and evaluating snow models at an Arctic site (Sodankyla, Finland). *Geoscientific Instrumentation, Methods and Data Systems*, *5*(1), 219–227. https://doi.org/10.5194/gi-5-219-2016

Essery, R., Morin, S., Lejeune, Y., & Ménard, C. B. (2013). A comparison of 1701 snow models using observations from an alpine site. *Advances in Water Resources*, *55*, 131–148. https://doi.org/10.1016/j.advwatres.2012.07.013

Essery, R., Pomeroy, J., Ellis, C., & Link, T. (2008). Modelling longwave radiation to snow beneath forest canopies using hemispherical photography or linear regression. *Hydrological Processes*, *22*, 2788–2800. https://doi.org/10.1002/hyp.6930

Essery, R., Rutter, N., Pomeroy, J., Baxter, R., Stähli, M., Gustafsson, D., et al. (2009). SnowMIP2: An evaluation of forest snow process simulation. *Bulletin of the American Meteorological Society*, *90*(8), 1130–1135. https://doi.org/10.1175/2009BAMS2629.1

Flanner, M. G., & Zender, C. S. (2005). Snowpack radiative heating: Influence on Tibetan Plateau climate. *Geophysical Research Letters*, *32*, L06501. https://doi.org/10.1029/2004GL022076

Froelich, N., Croft, H., Chen, J., Gonsamo, A., & Staebler, R. (2015). Trends of carbon fluxes and climate over a mixed temperate-boreal transition forest in southern Ontario, Canada. *Agricultural and Forest Meteorology*, *211-212*, 72–84. https://doi.org/10.1016/j.agrformet.2015.05.009

Gent, P. R., Danabasoglu, G., Donner, L. J., Holland, M. M., Hunke, E. C., Jayne, S. R., et al. (2011). The Community Climate System Model Version 4. *Journal of Climate*, *24*, 4973–4991. https://doi.org/10.1175/2011JCLI4083.1

Gouttevin, I., Lehning, M., Jonas, T., Gustafsson, D., & Mölder, M. (2015). A two-layer canopy model with thermal inertia for an improved snowpack energy balance below needleleaf forest (model SNOWPACK, version 3.2.1, revision 741). *Geoscientific Model Development*, *8*, 2379–2398. https://doi.org/10.5194/gmd-8-2379-2015

Hancock, S., Essery, R., Reid, T., Carle, J., Baxter, R., Rutter, N., & Huntley, B. (2014). Characterising forest gap fraction with terrestrial lidar and photography: An examination of relative limitations. *Agricultural and Forest Meteorology*, *189–190*, 105–114. https://doi.org/10.1016/j.agrformet.2014.01.012

Harding, R., & Pomeroy, J. (1996). The energy balance of the winter boreal landscape. *Journal of Climate*, *9*(11), 2778–2787. https://doi.org/10.1175/1520-0442(1996)009<2778:TEBOTW>2.0.CO;2

Henderson-Sellers, A., Pitman, A. J., Love, P. K., Irannejad, P., & Chen, T. H. (1995). The Project for Intercomparison of Land Surface Parameterization Schemes (PILPS): Phases 2 and 3. *Bulletin of the American Meteorological Society*, *76*(4), 489–503.

Howard, R., & Stull, R. (2013). IR radiation from trees to a ski run: A case study. *Journal of Applied Meteorology and Climatology*, *52*, 1525–1539. https://doi.org/10.1175/JAMC-D-12-0222.1

Lafaysse, M., Cluzet, B., Dumont, M., Lejeune, Y., Vionnet, V., & Morin, S. (2017). A multiphysical ensemble system of numerical snow modelling. *Cryosphere*, *11*(3), 1173–1198. https://doi.org/10.5194/tc-11-1173-2017

Link, T. E., & Marks, D. (1999). Point simulation of seasonal snow cover dynamics beneath boreal forest canopies. *Journal of Geophysical Research*, *104*, 27,841–27,857. https://doi.org/10.1029/1998JD200121

Lundquist, J. D., Dickerson-Lange, S. E., Lutz, J. A., & Cristea, N. C. (2013). Lower forest density enhances snow retention in regions with warmer winters: A global framework developed from plot-scale observations and modeling. *Water Resources Research*, *49*, 6356–6370. https://doi.org/10.1002/wrcr.20504

Mudryk, L. R., Kushner, P. J., & Derksen, C. (2014). Interpreting observed northern hemisphere snow trends with large ensembles of climate simulations. *Climate Dynamics*, *43*, 345–359. https://doi.org/10.1007/s00382-013-1954-y

Neumann, H., Den Hartog, G., & Shaw, R. (1989). Leaf area measurements based on hemispheric photographs and leaf-litter collection in a deciduous forest during autumn leaf-fall. *Agricultural and Forest Meteorology*, *45*(3-4), 325–345. https://doi.org/10.1016/0168-1923(89)90052-X

Ohta, T., Hiyama, T., Tanaka, H., Kuwada, T., Maximov, T., Ohata, T., & Fukushima, Y. (2001). Seasonal variation in the energy and water exchanges above and below a larch forest in eastern Siberia. *Hydrological Processes*, *15*(8), 1459–1476. https://doi.org/10.1002/hyp.219

Oleson, K., Lawrence, D., Bonan, G., Drewniak, B., Huang, M., Koven, C., et al. (2013). Technical description of version 4.5 of the Community Land Model (CLM). Boulder, CO: National Center for Atmospheric Research. https://doi.org/10.5065/D6RR1W7M

Pomeroy, J. W., Gray, D. M., Shook, K. R., Toth, B., Essery, R. L. H., Pietroniro, A., & Hedstrom, N. (1998). An evaluation of snow accumulation and ablation processes for land surface modelling. *Hydrological Processes*, *12*, 2339–2367. https://doi.org/10.1002/(SICI)1099-1085(199812)12:15<2339::AID-HYP800>3.0.CO;2-L

Pomeroy, J. W., Marks, D., Link, T., Ellis, C., Hardy, J., Rowlands, A., & Granger, R. (2009). The impact of coniferous forest temperature on incoming longwave radiation to melting snow. *Hydrological Processes*, *23*, 2513–2525. https://doi.org/10.1002/hyp.7325

Reid, T. D., Essery, R. L. H., Rutter, N., & King, M. (2014). Data-driven modelling of shortwave radiation transfer to snow through boreal birch and conifer canopies. *Hydrological Processes*, *28*(6), 2987–3007. https://doi.org/10.1002/hyp.9849

Reid, T., Spencer, M., Huntley, B., Hancock, S., Essery, R., Carle, J., et al. (2014). Spatial quantification of leafless canopy structure in a boreal birch forest. *Agricultural and Forest Meteorology*, *188*, 1–12. https://doi.org/10.1016/j.agrformet.2013.12.005

Rowlands, A., Pomeroy, J., Hardy, J., Marks, D., Elder, K., & Melloh, R. (2002). Small-scale spatial variability of radiant energy for snowmelt in a mid-latitude sub-alpine forest. In *Proceedings of the 59th Eastern Snow Conference*, Stowe, Vermont, USA, pp. 109–117. https://www.easternsnow.org/proceedings/2002/010_Rowlands.pdf

Rupp, D. E., Mote, P. W., Bindoff, N. L., Stott, P. A., & Robinson, D. A. (2013). Detection and attribution of observed changes in Northern Hemisphere spring snow cover. *Journal of Climate*, *26*, 6904–6914. https://doi.org/10.1175/JCLI-D-12-00563.1

Rutter, N., Essery, R., Pomeroy, J., Altimir, N., Andreadis, K., Baker, I., et al. (2009). Evaluation of forest snow processes models (SnowMIP2). *Journal of Geophysical Research*, *114*, D06111. https://doi.org/10.1029/2008JD011063

Sellers, P. J. (1985). Canopy reflectance, photosynthesis and transpiration. *International Journal of Remote Sensing*, *6*(8), 1335–1372. https://doi.org/10.1080/01431168508948283

Sicart, J. E., Pomeroy, J. W., Essery, R. L. H., Hardy, J., Link, T., & Marks, D. (2004). A sensitivity study of daytime net radiation during snowmelt to forest canopy and atmospheric conditions. *Journal of Hydrometeorology*, *5*(5), 774–784. https://doi.org/10.1175/1525-7541(2004)005<0774:ASSODN>2.0.CO;2

Stähli, M., Jonas, T., & Gustafsson, D. (2009). The role of snow interception in winter-time radiation processes of a coniferous sub-alpine forest. *Hydrological Processes*, *23*, 2498–2512. https://doi.org/10.1002/hyp.7180

Strasser, U., Warscher, M., & Liston, G. (2011). Modeling snow-canopy processes on an idealized mountain. *Journal of Hydrometeorology*, *12*(4), 663–677. https://doi.org/10.1175/2011JHM1344.1

Teklemariam, T., Staebler, R., & Barr, A. (2009). Eight years of carbon dioxide exchange above a mixed forest at Borden, Ontario. *Agricultural and Forest Meteorology*, *149*(11), 2040–2053. https://doi.org/10.1016/j.agrformet.2009.07.011

Thackeray, C. W., Fletcher, C. G., & Derksen, C. (2014). The influence of canopy snow parameterizations on snow albedo feedback in boreal forest regions. *Journal of Geophysical Research: Atmospheres*, *119*, 9810–9821. https://doi.org/10.1002/2014JD021858

Thackeray, C. W., Fletcher, C. G., Mudryk, L. R., & Derksen, C. (2016). Quantifying the uncertainty in historical and future simulations of Northern Hemisphere spring snow cover. *Journal of Climate*, *29*(23), 8647–8663. https://doi.org/10.1175/JCLI-D-16-0341.1

Webster, C., Rutter, N., Zahner, F., & Jonas, T. (2016a). Modeling subcanopy incoming longwave radiation to seasonal snow using air and tree trunk temperatures. *Journal of Geophysical Research: Atmospheres*, *121*, 1220–1235. https://doi.org/10.1002/2015JD024099

Webster, C., Rutter, N., Zahner, F., & Jonas, T. (2016b). Measurement of incoming radiation below forest canopies: A comparison of different radiometer configurations. *Journal of Hydrometeorology*, *17*, 853–864. https://doi.org/10.1175/JHM-D-15-0125.1

Woo, M., & Giesbrecht, M. A. (2000). Simulation of snowmelt in a subarctic spruce woodland: 1. Tree model. *Water Resources Research*, *36*(8), 2275–2285. https://doi.org/10.1029/2000WR900094

Zweifel, R., Haeni, M., Buchmann, N., & Eugster, W. (2016). Are trees able to grow in periods of stem shrinkage? *New Phytologist*, *211*(3), 839–849. https://doi.org/10.1111/nph.13995